



LETTER | MAY 23 2024


## Directly driven magnetized fast-ignition targets with steep density gradients for inertial fusion energy

A. B. Sefkow ; B. G. Logan; M. Tabak 



*Phys. Plasmas* 31, 050704 (2024)


<https://doi.org/10.1063/5.0197817>



### APL Machine Learning

2023 Papers with Best Practices in Data Sharing and Comprehensive Background

[Read Now](#)



# Directly driven magnetized fast-ignition targets with steep density gradients for inertial fusion energy

Cite as: Phys. Plasmas **31**, 050704 (2024); doi: 10.1063/5.0197817

Submitted: 14 January 2024 · Accepted: 25 March 2024 ·

Published Online: 23 May 2024



View Online



Export Citation



CrossMark

A. B. Sefkow,<sup>1,2,3,4,a)</sup>  B. C. Logan,<sup>5</sup> and M. Tabak<sup>6</sup> 

## AFFILIATIONS

<sup>1</sup>Department of Mechanical Engineering, University of Rochester, Rochester, New York 14627, USA

<sup>2</sup>Department of Physics and Astronomy, University of Rochester, Rochester, New York 14627, USA

<sup>3</sup>Department of Computer Science, University of Rochester, Rochester, New York 14627, USA

<sup>4</sup>Laboratory for Laser Energetics, University of Rochester, Rochester, New York 14623, USA

<sup>5</sup>Lawrence Berkeley National Laboratory, Berkeley, California 94720, USA

<sup>6</sup>Lawrence Livermore National Laboratory, Livermore, California 94550, USA

<sup>a)</sup>Author to whom correspondence should be addressed: [adam.sefkow@rochester.edu](mailto:adam.sefkow@rochester.edu)

## ABSTRACT

The development of advanced targets capable of achieving ignition with improved energy gain at lower driver energies is one of four key technical challenges to be solved in order to realize economical inertial fusion energy. We report the minimum energy necessary for a small hemispherical mass of fast-ignited high-density deuterium–tritium fuel to explosively ignite a significantly larger hemispherical mass of assembled cold fuel with much lower mass density, both with and without a flux-compressed magnetic field connecting the two regions. With the magnetic field, the burn rate improves, and lower energy states become more effective. The imploded fuel reservoir available in the lower-density, larger-mass region of the steep density gradient determines whether the fusion yield is several hundred MJ or up to a few GJ. We report a case wherein the cold reservoir ignited and produced high gain with the assistance of only  $\sim 700$  kJ of hotspot yield, an amount that has already been demonstrated as feasible in laboratory experiments using indirect-drive targets.

© 2024 Author(s). All article content, except where otherwise noted, is licensed under a Creative Commons Attribution (CC BY) license (<https://creativecommons.org/licenses/by/4.0/>). <https://doi.org/10.1063/5.0197817>

In the inertial confinement fusion (ICF) approach to the production of thermonuclear plasma in the laboratory, many lasers are used to symmetrically compress a capsule containing fusion fuel into the burning-plasma regime.<sup>1</sup> In order to reach that state, a minimum ignition ion temperature  $T_i$  and areal density  $\rho R$  must be achieved such that the triple product  $\rho R T_i \geq 5$  keV g/cm<sup>2</sup> with  $T_i \geq 4$  keV. Experiments at the National Ignition Facility (NIF) located at Lawrence Livermore National Laboratory (LLNL) have demonstrated the achievement of this state,<sup>2</sup> resulting in several MJ of fusion yield, and, hence, have spurred a renewed interest in an inertial fusion energy (IFE) program in the US and around the world.

The ultimate goal of developing economically attractive IFE power plants requires the accelerated development of four grand challenges:<sup>3–5</sup> (1) demonstration of the achievement of ICF ignition in the laboratory (now complete), (2) production of advanced high-gain targets and drivers for them, (3) creation of a practical thermonuclear

fusion engine, and (4) development of economical fusion power plants with reduced target and driver costs. Advanced fast-ignition targets, in which the compression and ignition phases are separated, may lower the energy requirements to ignite<sup>6</sup> using advanced drivers capable of high repetition rate, high efficiency, and high average powers. With the improvement of current experimental performance, a practical fusion engine may be realized and eventually lead to economical power from IFE. Significant cost reductions can be achieved through substantial improvements in the performance of targets, in other words the achievement of high gain at reduced ignition energy while minimizing the per-target cost. Reducing driver costs by inventing higher performance targets is necessary but not sufficient for the commercial success of IFE.<sup>3</sup>

An advanced target concept to achieve high-gain performance was recently proposed<sup>3,4</sup> in which a small hemispherical mass of high-density, fast-ignited deuterium–tritium (DT) is used to ignite a much

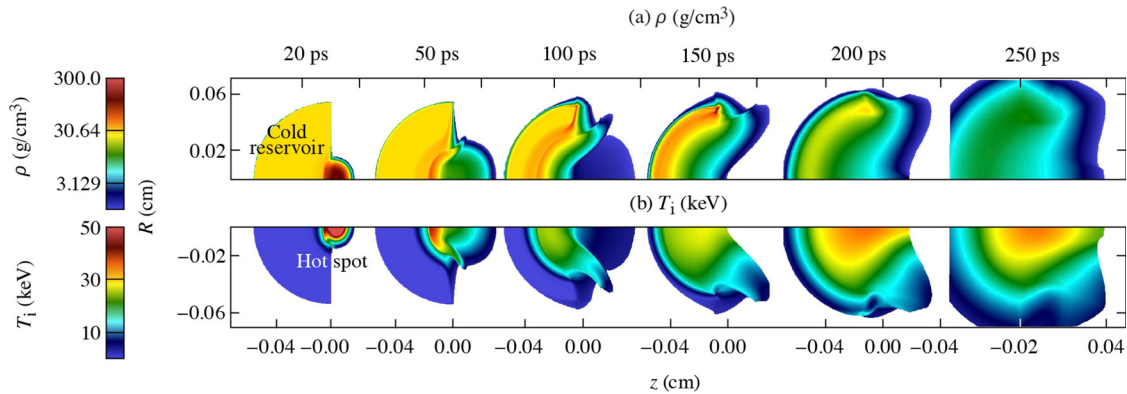


**FIG. 1.** The small mass of high-density DT fuel explosively ignites the larger mass of fuel. (a) Mass density  $\rho$  on a log scale from 1 to 300  $\text{g}/\text{cm}^3$ . (b) Ion temperature  $T_i$  on a linear scale from 0 to 50 keV. Fast electrons (not shown) would be injected into the hot spot from the right, possibly using a cone for guiding.

larger hemispherical mass of low-density DT. The ignition process is characterized by a self-heating thermonuclear burn wave that radially propagates down the density gradient from the hotspot region into cold surrounding fuel layers, resulting in more fusion energy output than was absorbed by the capsule.<sup>7</sup> Calculations suggested the assembly may yield several hundred MJ of fusion energy when directly driven into its stagnated state, and an ignitor pulse is used to initiate the burn wave.<sup>4</sup> Other work has also studied the use of hemispherical targets in fast-ignition and pulsed-power ICF.<sup>8–10</sup>

This work investigates two new improvement areas for high-gain ignition using a steep density gradient, beyond the original paper by Nuckolls (Ref. 4). We explore a range of assembled masses, mass densities, and areal densities in order to inform minimum ignition energy requirements for future integrated simulations. We also evaluate the benefit of a compressed  $B_z$  field connecting the two hemispheres of different fuel densities and quantify the improvement from its use.

The original simulation used two hemispherical masses of DT fuel,<sup>4</sup> referred to here as the hotspot and the cold reservoir. The purpose of the cold reservoir is to independently control and produce a higher yield and gain due to the extra mass present. The initial configuration for the calculation of ignition across a tenfold density step is as follows. The cold reservoir has lower compressed mass density than the hotspot, where  $\rho_c = 30 \text{ g}/\text{cm}^3$  and  $\rho_{hs} = 300 \text{ g}/\text{cm}^3$ , respectively, and both are assumed to have been isochorically assembled.<sup>11</sup> The hotspot is the fast-ignited hemispherical mass with radius  $R_{hs} = 100 \mu\text{m}$  containing  $\rho R_{hs} = 3 \text{ g}/\text{cm}^2$  at a temperature of  $k_B T = 10 \text{ keV}$ , giving an energy contained of 1.01 MJ. The cold reservoir into which the burning hotspot will radially propagate has a radius of  $R_c = 540 \mu\text{m}$  containing  $\rho R_c = 1.6 \text{ g}/\text{cm}^2$  at a temperature of  $k_B T = 100 \text{ eV}$ , giving an energy contained of 110 kJ. The mass ratio is  $m_c/m_{hs} = 16$ . We note the text and associated figure of the initial configuration provided in Ref. 4 did not agree, and we assumed the figure was correct ( $16\times$  larger mass rather than  $10\times$  in the text, and  $\rho R_c = 1.6 \text{ g}/\text{cm}^2$  rather than  $\rho R_c = 1.4 \text{ g}/\text{cm}^2$  in the text).

Figure 1 illustrates the radial propagation of the burn wave within the two hemispheres at the times shown. Although the cold reservoir does burn some of its DT fuel, while the hotspot transfers energy to it through thermal conduction, radiation, and alpha-particle deposition, it does not ignite until 50 ps has elapsed. At that point, a shock wave

and its precursor propagate throughout the reservoir due to radiation and alphas. There is no imposed magnetic field in this case. The ion temperature of this robustly burning target reaches about 35 keV at late time and has an elongated shape, in agreement with the previous work.<sup>4</sup> Note the density plot cutoff used is  $1 \text{ g}/\text{cm}^3$ , so the plots outline that contour.

Two distinct episodes of burn can be seen to exist within the target. The hotspot peak thermonuclear energy production rate at 10 ps is about 3 MJ/ps during its burn, similar to the peak of about 4 MJ/ps attained around 150 ps by the cold fuel reservoir, as shown in Fig. 2. Note the log–log scale and the fact that the cold fuel burns for much longer due to its higher mass and cooler temperature achieved during ignition (the peak hotspot ion temperature exceeds  $k_B T_i = 50 \text{ keV}$ ). The fast-ignited hemispherical target achieves a total fusion gain of 400 MJ, relevant for an IFE power plant, where the majority of that

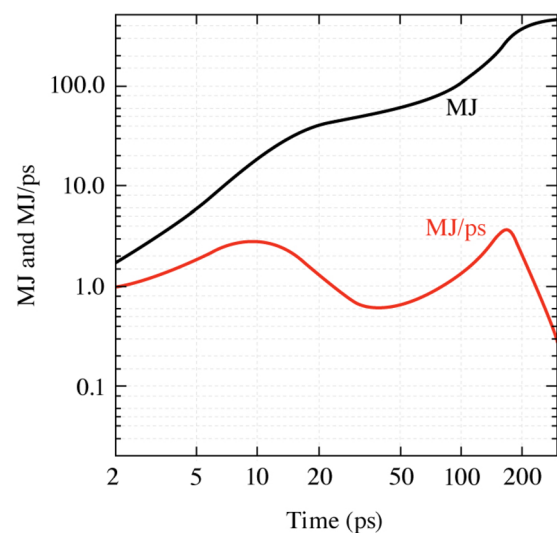


**FIG. 2.** The burn history of the robustly burning benchmark case. The total fusion energy produced is plotted in black in units of MJ, and the fusion energy production rate is in red in units of MJ/ps. Note the log–log scale. The hotspot produces about 30 MJ, and the cold reservoir produces about 400 MJ of fusion energy.

05 June 2024 14:26:48

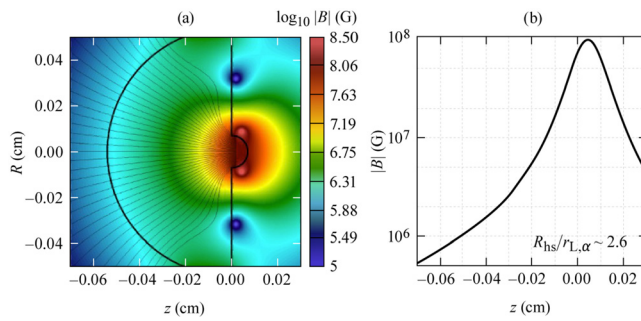


**FIG. 3.** The assumed magnetic-field topology for the simulations in this paper. (a) The field has been flux-compressed to the  $\sim 100$ -MG level, with field lines connecting the hot spot to the adjacent cold fuel reservoir. The RZ plot is plotted twice with one half flipped for clarity of illustration. The field lines have only been plotted in the cold fuel, also for clarity. (b) Lineout of  $B_z$  along  $R=0$ .

yield originated in the cold fuel region. In other words, the fast ignition of the hotspot in a steep density gradient enabled IFE-relevant fusion energy gains from a more modestly driven direct-drive target ( $\rho_c = 30 \text{ g/cm}^3$ ).

Next, we assume an imposed magnetic field has been flux-compressed to the  $\sim 100$ -MG level with field lines connecting the hot spot to the adjacent cold fuel reservoir. Magnetic fields are known to be able to increase yields in fusion targets due to suppressed electron thermal conduction losses, and thus elevated temperatures during the implosion and at stagnation.<sup>12–19</sup> The 100-MG strength is the order of magnitude required to marginally magnetize the fusion-produced alpha particles and trap some of their energy in the hotspot, if and when the  $\rho R$  is insufficient,<sup>13,20,21</sup> but it is not so high as to impede the burn propagation.<sup>22,23</sup> Earlier work showed B fields at this level can degrade hot electron coupling due to magnetic mirroring.<sup>24</sup> Our goal in comparing magnetized to unmagnetized variants of the fast-ignited steep density gradient target will be to quantify the benefit of the magnetic field on achieving ignition, such as the improvement of the ignition cliff.<sup>25</sup> The assumed magnetic-field topology initialized at stagnation ( $t=0$  of the simulation) is depicted in Fig. 3. The corresponding value of  $R_{hs}/r_{L,\alpha}$  achieves a maximum value of 2.6, where  $R_{hs}$  is the radius of the hotspot and  $r_{L,\alpha}$  is the Larmor radius of the fusion-produced alpha particles. Values greater than 1 indicate the hotspot is larger in radius than the Larmor radius; therefore, alpha particles will deposit most of their energy in the nearby hot area.<sup>20</sup> Although the magnetic field helps transport alpha particle energy to the cold reservoir, the dominant effect of the magnetic field is the suppression of heat conduction losses causing the target to stay hotter.

In particular, we seek to lower the energy investment into the hotspot to well below 1 MJ and operate closer to the ignition cliff than the benchmarked case discussed earlier. We also seek to reduce the density gradient from tenfold to just a several-fold change in order to relax the hydrodynamic assembly issues with being out of pressure equilibrium. To do so, we ran a series of simulations to determine the ignition cliff and its dependence on the high-density hotspot  $\rho_{hs}$  and  $\rho R_{hs} T_i$ , the fusion triple product responsible for determining whether or not a capsule will ignite. We also investigated several values of  $\rho_c$ ,  $\rho R_c$ , and the mass ratio of the hemispherical regions  $m_c/m_{hs}$ .

The results of our parameter sensitivity study on the ignition cliff of the magnetized targets are reported in Table I. Three sets of cold

**TABLE I.** Parameters involved in the burn sensitivity study:  $\rho_c$  and  $\rho R_c$  are the mass and areal densities of the cold fuel reservoir,  $\rho_{hs}$  and  $\rho R_{hs}$  are the mass and areal densities of the hot spot,  $m_c/m_{hs}$  is the mass ratio of the two hemispheres,  $\rho R_{hs} T_i$  is the initial triple product of the hot spot,  $E_{hs}^0$  is the initial hot spot energy, and  $I_{flag}$  denotes whether the target ignited or not.

$\rho_c$ (g/cm <sup>3</sup> )	$\rho R_c$ (g/cm <sup>2</sup> )	$\rho_{hs}$ (g/cm <sup>3</sup> )	$\rho R_{hs}$ (g/cm <sup>2</sup> )	$m_c/m_{hs}$	$\rho R_{hs} T_i$ (g/cm <sup>2</sup> keV)	$E_{hs}^0$ (kJ)	$I_{flag}^a$
30	1.6	280	1.96	49	11.8	150	1
30	1.6	260	1.82	53	10.9	140	*
30	1.6	240	1.68	57	10.1	130	*
30	1.6	220	1.54	63	9.2	120	0
30	1.6	200	1.40	69	8.4	110	0
60	3.2	280	1.96	98	11.8	150	1
60	3.2	260	1.82	106	10.9	140	1
60	3.2	240	1.68	115	10.1	130	1
60	3.2	220	1.54	125	9.2	120	1
60	3.2	200	1.40	138	8.4	110	1
60	3.2	180	1.26	153	7.6	100	*
60	3.2	160	1.12	172	6.7	90	0
60	3.2	140	0.98	197	5.9	80	0
60	3.2	120	0.84	230	5.0	70	0
60	3.2	100	0.70	275	4.2	60	0
90	4.9	280	1.96	148	11.8	150	1
90	4.9	260	1.82	159	10.9	140	1
90	4.9	240	1.68	172	10.1	130	1
90	4.9	220	1.54	189	9.2	120	1
90	4.9	200	1.40	207	8.4	110	1
90	4.9	180	1.26	230	7.6	100	1
90	4.9	160	1.12	258	6.7	90	*
90	4.9	140	0.98	295	5.9	80	*
90	4.9	120	0.84	344	5.0	70	0
90	4.9	100	0.70	413	4.2	60	0

<sup>a</sup>The ignition flag  $I_{flag}$  denotes whether the cold reservoir ignites (1), fails to ignite (0), or if it ignites with the magnetic field but not without it (\*).

fuel reservoir mass densities and areal densities were investigated, namely,  $\rho_c = 30 \text{ g/cm}^3$  ( $\rho R_c = 1.6 \text{ g/cm}^2$ ),  $60 \text{ g/cm}^3$  ( $\rho R_c = 3.2 \text{ g/cm}^2$ ), and  $90 \text{ g/cm}^3$  ( $\rho R_c = 4.9 \text{ g/cm}^2$ ). The cold fuel reservoir was assumed to have been isochorically assembled on a low adiabat,<sup>11</sup> with an estimated temperature at stagnation of  $k_B T = 10 \text{ eV}$ , corresponding to initial energies of 21, 68, and 135 kJ for the three mass densities; starting with a higher temperature than 10 eV increases the initial absorbed energy but the cold fuel still ignites. Ignition is defined as whether the cold reservoir of fuel achieved a burn rate comparable to the hotspot, such that half or more of the total yield originated from the larger cold fuel mass. For each cold reservoir case, the hotspot mass densities and areal densities were then decremented from  $\rho_{hs} = 280$  to  $100 \text{ g/cm}^3$  by  $20 \text{ g/cm}^3$  at a time until the target failed to ignite. The hotspot radius and temperature were both fixed at  $R_{hs} = 70 \text{ }\mu\text{m}$  and  $k_B T = 6 \text{ keV}$ , respectively, which were lower than the values of  $100 \text{ }\mu\text{m}$  and  $10 \text{ keV}$  in the original calculation of Ref. 4. Both magnetized and unmagnetized variants were simulated.

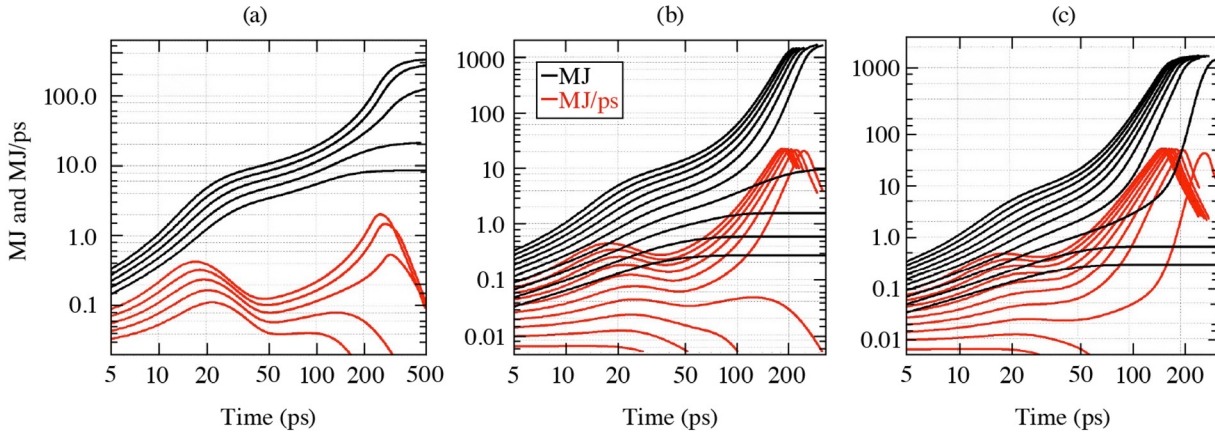


**FIG. 4.** The burn histories for the magnetized target parameter scans. The total fusion energy produced is plotted in black in units of MJ, and the fusion energy production rate is in red in units of MJ/ps. Note the log–log scale. Cases used a cold reservoir mass density of (a)  $\rho_c = 30$ , (b)  $\rho_c = 60$ , or (c)  $\rho_c = 90 \text{ g/cm}^3$  corresponding to areal densities of  $\rho R = 1.6, 3.2,$  and  $4.9 \text{ g/cm}^2$ , respectively. Each curve has a corresponding entry in Table I. The top curves in each plot are the  $\rho_{hs} = 280 \text{ g/cm}^3$  cases, and each subsequent curve decrements the mass density by  $20 \text{ g/cm}^3$ .

Targets with larger  $\rho_{hs}$  and  $\rho R_{hs}$  burned more robustly and with more margin. Generally, it was found that the magnetized targets shared the burn-performance characteristics of the unmagnetized cases that were about  $\rho_{hs} = 40 \text{ g/cm}^3$  higher, indicating that the magnetic field plays a helpful role in improving the margin and gain, in agreement with other studies.<sup>25</sup> The minimum  $\rho R_{hs} T_i$  triple product required to ignite was shown to be a function of the cold reservoir parameters, varying from  $10.1$  to  $5.9 \text{ g/cm}^2 \text{ keV}$  for  $\rho_c = 30$  to  $90 \text{ g/cm}^3$ , respectively. The results are consistent with other work that showed  $5.0 \text{ g/cm}^2 \text{ keV}$  to be a hard lower bound for achieving ignition in conventional ICF.<sup>26</sup>

For each case presented in Table I, a corresponding temporal burn history plot has been provided in Fig. 4. The curves from top to bottom are in the same order as they are presented in Table I, with the top curve belonging to the  $\rho_{hs} = 280 \text{ g/cm}^3$  case. Each case is the magnetized variant. As the hotspot mass density is lowered while keeping the radius and temperature fixed, the yield from the cold fuel reservoir is delayed in time until it no longer ignites. If the IFE-relevant multi-hundred MJ or several GJ yields are not desirable, one could simply alter the desired stagnation state of the cold fuel reservoir to utilize lower radius and areal density. Again, the unmagnetized variants have similar burn histories as the magnetized cases but with  $40 \text{ g/cm}^3$  higher initial hotspot mass density. Table I indicates whether a given unmagnetized version failed to ignite.

Both the magnetized and unmagnetized versions of the  $\rho_c = 90 \text{ g/cm}^3$  and  $\rho_{hs} = 180 \text{ g/cm}^3$  case ignited, with an initial hotspot energy of  $100 \text{ kJ}$ . In order to study the sensitivity to the fast-ignition deposited power, we revisited this case but did not initialize the hotspot temperature at  $6 \text{ keV}$ . Instead, power was deposited into the initially cold hotspot at a rate of  $10, 4,$  and  $3 \text{ PW}$ , corresponding to  $100 \text{ kJ}$  in  $10, 25,$  and  $33 \text{ ps}$ , respectively. As depicted in Fig. 5, the magnetized cases burn faster than their unmagnetized counterparts. Also,  $4 \text{ PW}$  was the cutoff for ignition in the unmagnetized case, whereas it was  $3 \text{ PW}$  with the field.

Of particular interest is the magnetized case near the ignition cliff using  $\rho_c = 90 \text{ g/cm}^3$ ,  $\rho R_c = 4.9 \text{ g/cm}^2$ ,  $\rho_{hs} = 140 \text{ g/cm}^3$ , and  $\rho R_{hs} = 0.98 \text{ g/cm}^2$ , with  $k_B T_c = 10 \text{ eV}$  and  $k_B T_{hs} = 6 \text{ keV}$ . The cold reservoir absorbed  $135 \text{ kJ}$ , and the hotspot initial energy was only  $80 \text{ kJ}$ . The

energetics of this  $m_c/m_{hs} \sim 300$  assembly are illustrated in Fig. 6. We define the time of ignition of the cold fuel reservoir to be the time when half the energy from fusion burn was produced from the cold mass rather than the hot spot, and so the total fusion energy has approximately doubled compared to the hot spot burn alone. In this case, ignition occurs about  $65 \text{ ps}$  after the hotspot has started burning. About  $280 \text{ kJ}$  of fusion-produced alpha-particle energy has been produced at this point;  $\sim 140 \text{ kJ}$  of alpha energy from the hotspot has been generated, and about half of the alphas have deposited their energy

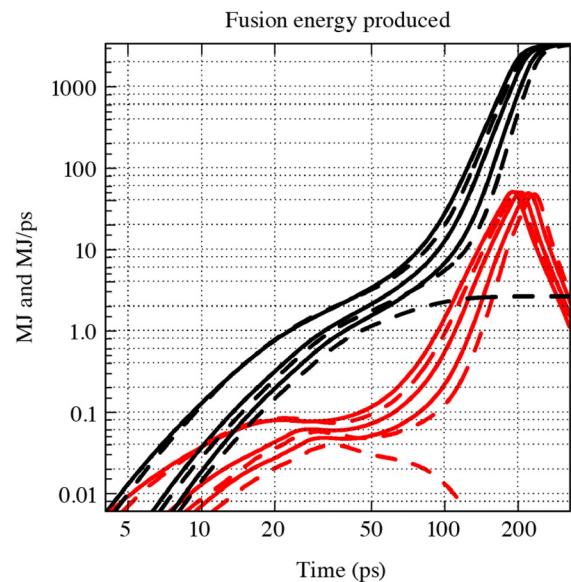


**FIG. 5.** The burn histories for the cases  $\rho_c = 90 \text{ g/cm}^3$  and  $\rho_{hs} = 180 \text{ g/cm}^3$  with varying deposited powers both (solid) with magnetic field and (dashed) without magnetic field. The total fusion energy produced is plotted in black in units of MJ and the fusion energy production rate is in red in units of MJ/ps. Note the log–log scale. The cases correspond to fast-ignition heating rates of  $10, 4,$  and  $3 \text{ PW}$ , from top to bottom.

05 June 2024 14:26:48

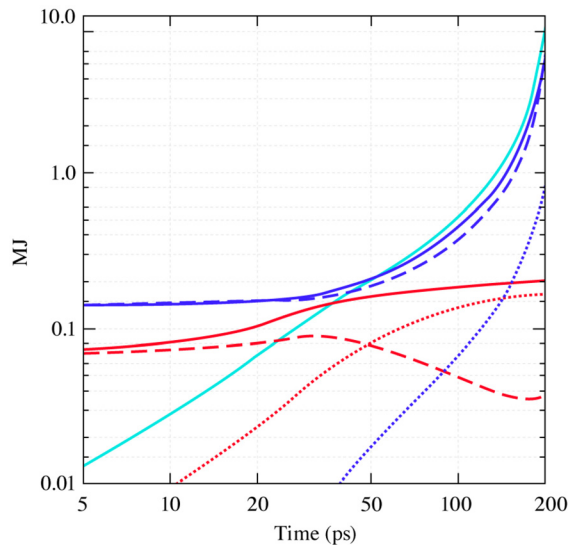


**FIG. 6.** Energetics of the capsule near the ignition cliff for the case  $\rho_c = 90 \text{ g/cm}^3$  and  $\rho R_c = 4.9 \text{ g/cm}^2$ . The cold fuel (blue) total energy (solid), internal energy (dashed), and kinetic energy (dotted) are compared to the hot spot (red) total energy (solid), internal energy (dashed), and kinetic energy (dotted), respectively. Also shown is the alpha particle energy produced (cyan) by fusion. This case is also listed as the third from the end in Table I.

into the cold fuel (the other half flows the other direction due to the magnetic field). Since 80% of the DT fusion energy is carried away by energetic neutrons without much interaction in the fuel, an approximate fusion yield of  $\sim 700 \text{ kJ}$  was needed from the  $\rho_{\text{hs}} = 140 \text{ g/cm}^3$  hotspot to initiate radial propagation of the burn wave into the surrounding cold fuel reservoir. The unmagnetized variant did not ignite.

The original published design<sup>1</sup> required 1.12 MJ total absorbed energy to form the stagnated state for the subsequent burn calculation; 110 kJ absorbed in a cold fuel reservoir of  $\rho_c = 30 \text{ g/cm}^3$  with  $\rho R_c = 1.6 \text{ g/cm}^2$  and 1.01 MJ absorbed in a  $\rho_{\text{hs}} = 300 \text{ g/cm}^3$  hotspot with  $\rho R_{\text{hs}} = 3.0 \text{ g/cm}^2$  and  $k_B T = 10 \text{ keV}$ . The total yield of  $\sim 450 \text{ MJ}$  required about 50 MJ from the hotspot to initiate burn in the reservoir. Here, we have identified a design requiring only 80 kJ absorbed in a  $\rho_{\text{hs}} = 140 \text{ g/cm}^3$  hotspot with  $\rho R_{\text{hs}} = 1.0 \text{ g/cm}^2$  and  $k_B T = 6 \text{ keV}$ . The cold reservoir ignited with IFE-relevant gains with the assistance of  $\sim 700 \text{ kJ}$  of hotspot yield, an amount that has already been demonstrated as feasible on the NIF at LLNL using indirect-drive targets.<sup>2</sup> Since direct-drive targets are more efficient, such a state is also likely achievable.

The author (ABS) thanks J. H. Nuckolls and A. L. Velikovich for useful comments and suggestions. This material is based upon work supported by the U.S. DOE OFES under Award No. DE-SC0017951, the U.S. DOE ARPA-E under Award No. DE-AR0001272, and the U.S. DOE NNSA University of Rochester “National Inertial Confinement Program” under Award No. DE-NA0004144. This report was prepared as an account of work sponsored by an agency of the U.S. Government. Neither the U.S. Government nor any agency thereof, nor any of their employees, makes any warranty, express or implied, or assumes any legal liability or responsibility for the accuracy, completeness, or usefulness of any information, apparatus, product, or process disclosed, or represents that its use would not infringe privately owned rights.

Reference herein to any specific commercial product, process, or service by trade name, trademark, manufacturer, or otherwise does not necessarily constitute or imply its endorsement, recommendation, or favoring by the U.S. Government or any agency thereof. The views and opinions of authors expressed herein do not necessarily state or reflect those of the U.S. Government or any agency thereof.

## AUTHOR DECLARATIONS

### Conflict of Interest

The authors have no conflicts to disclose.

### Author Contributions

**A. B. Sefkow:** Conceptualization (lead); Formal analysis (lead); Software (lead); Writing – original draft (lead). **B. G. Logan:** Conceptualization (equal); Formal analysis (equal); Writing – review & editing (supporting). **M. Tabak:** Conceptualization (equal); Formal analysis (equal); Writing – review & editing (supporting).

## DATA AVAILABILITY

The data that support the findings of this study are available from the corresponding author upon reasonable request.

## APPENDIX: NUMERICAL METHODS

The TriForce code is under development to become a fluid-kinetic hybrid multiphysics model.<sup>27</sup> The fluid half of the code, named TFLUID, was used herein and is a radiation-hydrodynamics code for simulating ICF and high-energy-density-physics experiments. The model was two-dimensional and used an Eulerian prescription for solving the mass, momentum, and energy-conservation equations as well as the radiation transport.<sup>28</sup> Laser ray tracing was not included since the stagnated state was assumed as the initial condition. Resistive magnetohydrodynamics (MHD) uses an induction equation and simple Ohm’s law to impose and evolve the initial magnetic field. Also employed were electron thermal conduction, flux-limited multigroup radiation diffusion, thermonuclear reactions and multigroup diffusion for the resulting charged particles, and LEOS equation of state for the material (DT).<sup>29</sup> The conductivity and fusion burn models include anisotropic transport effects by using Epperlein–Haines corrections to the Braginskii transport coefficients.<sup>30</sup> Nonlocal transport corrections due to long mean free path effects are not included. Nonlinear laser–plasma interaction processes such as stimulated Brillouin and stimulated Raman scattering, two-plasmon decay, or filamentation<sup>31</sup> are also not included since the compression lasers and ignitor laser are not directly modeled in this work. The kinetic half of the TriForce code, named TFLINK, was not coupled, and a fully integrated fast-ignition simulation is left for future work.

## REFERENCES

- J. H. Nuckolls, L. Wood, A. Thiessen, and G. B. Zimmerman, “Laser compression of matter to super-high densities: Thermonuclear applications,” *Nature* **239**, 139–142 (1972).
- A. L. Kritcher, C. V. Young, H. F. Robey, C. R. Weber, A. B. Zylstra, O. A. Hurricane, D. A. Callahan, J. E. Ralph, J. S. Ross, K. L. Baker *et al.*, “Design of inertial fusion implosions reaching the burning plasma regime,” *Nat. Phys.* **18**, 251–258 (2022).

- <sup>3</sup>J. H. Nuckolls and L. L. Wood, "Future of inertial fusion energy," in 11th International Conference on Emerging Nuclear Energy Systems (ICENES), Albuquerque, NM, 20 September–4 October, 2002.
- <sup>4</sup>J. H. Nuckolls, "Grand challenges of inertial fusion energy," *J. Phys.: Conf. Ser.* **244**, 012007 (2010).
- <sup>5</sup>National Academies of Sciences, Engineering, and Medicine, *Plasma Science: Enabling Technology, Sustainability, Security, and Exploration* (The National Academies Press, Washington, DC, 2021).
- <sup>6</sup>M. Tabak, J. Hammer, M. E. Glinsky, W. L. Kruer, S. C. Wilks, J. Woodworth, E. M. Cambell, M. D. Perry, and R. J. Mason, "Ignition and high gain with ultrapowerful lasers," *Phys. Plasmas* **1**, 1626–1634 (1994).
- <sup>7</sup>M. Tabak, D. S. Clark, R. P. J. Town, and S. Hatchett, "Hydrodynamic assembly for fast ignition," in *49th Annual Meeting of the Division of Plasma Physics*, Orlando, FL, 12–16 November 2007 (Bulletin of the American Physical Society, 2007).
- <sup>8</sup>T. A. Mehlhorn, J. E. Bailey, G. Bennett, G. A. Chandler, G. Cooper, M. E. Cuneo, I. Golovkin, D. L. Hanson, R. J. Leeper, and J. J. MacFarlane, "Recent experimental results on ICF target implosions by Z-pinch radiation sources and their relevance to ICF ignition studies," *Plasma Phys. Controlled Fusion* **45**, A325 (2003).
- <sup>9</sup>M. K. Matzen, M. A. Sweeney, R. G. Adams, J. R. Asay, J. E. Bailey, G. R. Bennett, D. E. Bliss, D. D. Bloomquist, T. A. Brunner, R. B. Campbell *et al.*, "Pulsed-power-driven high energy density physics and inertial confinement fusion research," *Phys. Plasmas* **12**, 055503 (2005).
- <sup>10</sup>M. Temporal, "Fast ignition of a compressed inertial confinement fusion hemispherical capsule by two proton beams," *Phys. Plasmas* **13**, 122704 (2006).
- <sup>11</sup>D. S. Clark and M. Tabak, "A self-similar isochoric implosion for fast ignition," *Nucl. Fusion* **47**, 1147–1156 (2007).
- <sup>12</sup>P. Y. Chang, G. Fiksel, M. Hohenberger, J. P. Knauer, R. Betti, F. J. Marshall, D. D. Meyerhofer, F. H. Séguin, and R. D. Petrasso, "Fusion yield enhancement in magnetized laser-driven implosions," *Phys. Rev. Lett.* **107**, 035006 (2011).
- <sup>13</sup>A. B. Sefkow, S. A. Slutz, J. M. Koning, M. M. Marinak, K. J. Peterson, D. B. Sinars, and R. A. Vesey, "Design of magnetized liner inertial fusion experiments using the Z facility," *Phys. Plasmas* **21**, 072711 (2014).
- <sup>14</sup>M. R. Gomez, S. A. Slutz, A. B. Sefkow, D. B. Sinars, K. D. Hahn, S. B. Hansen, E. C. Harding, P. F. Knapp, P. F. Schmit, C. A. Jennings *et al.*, "Experimental demonstration of fusion-relevant conditions in magnetized liner inertial fusion," *Phys. Rev. Lett.* **113**, 155003 (2014).
- <sup>15</sup>W.-M. Wang, P. Gibbon, Z.-M. Sheng, and Y.-T. Li, "Magnetically assisted fast ignition," *Phys. Rev. Lett.* **114**, 015001 (2015).
- <sup>16</sup>J. D. Moody, A. Johnson, J. Javedani, E. Carroll, J. Fry, B. Koziemiński, S. O. Kucheyev, B. G. Logan, B. B. Pollock, H. Sio *et al.*, "Transient magnetic field diffusion considerations relevant to magnetically assisted indirect drive inertial confinement fusion," *Phys. Plasmas* **27**, 112711 (2020).
- <sup>17</sup>J. D. Moody, B. B. Pollock, H. Sio, D. J. Strozzi, D. D.-M. Ho, C. A. Walsh, G. E. Kemp, B. Lahmann, S. O. Kucheyev, B. Koziemiński *et al.*, "Increased ion temperature and neutron yield observed in magnetized indirectly driven D<sub>2</sub>-filled capsule implosions on the National Ignition Facility," *Phys. Rev. Lett.* **129**, 195002 (2022).
- <sup>18</sup>J. D. Moody, B. B. Pollock, H. Sio, D. J. Strozzi, D. D.-M. Ho, C. Walsh, G. E. Kemp, S. O. Kucheyev, B. Koziemiński, E. G. Carroll *et al.*, "The magnetized indirect drive project on the National Ignition Facility," *J. Fusion Energy* **41**, 7 (2022).
- <sup>19</sup>H. Sio, J. D. Moody, B. B. Pollock, D. Strozzi, D. D.-M. Ho, C. A. Walsh, G. E. Kemp, B. Lahmann, S. O. Kucheyev, B. Koziemiński *et al.*, "The magnetized indirect drive project on the National Ignition Facility," *Phys. Plasmas* **30**, 072709 (2023).
- <sup>20</sup>M. M. Basko, A. J. Kemp, and J. Meyer-ter-Vehn, "Ignition conditions for magnetized target fusion in cylindrical geometry," *Nucl. Fusion* **40**, 59 (2000).
- <sup>21</sup>P. F. Schmit, P. F. Knapp, S. B. Hansen, M. R. Gomez, K. D. Hahn, D. B. Sinars, K. J. Peterson, S. A. Slutz, A. B. Sefkow, T. J. Awe *et al.*, "Understanding fuel magnetization and mix using secondary nuclear reactions in magneto-inertial fusion," *Phys. Rev. Lett.* **113**, 155004 (2014).
- <sup>22</sup>S. A. Slutz and R. A. Vesey, "High-gain magnetized inertial fusion," *Phys. Rev. Lett.* **108**, 025003 (2012).
- <sup>23</sup>B. Appelbe, A. L. Velikovich, M. Sherlock, C. Walsh, A. Crilly, S. O'Neill, and J. Chittenden, "Magnetic field transport in propagating thermonuclear burn," *Phys. Plasmas* **28**, 032705 (2021).
- <sup>24</sup>D. J. Strozzi, M. Tabak, D. J. Larson, L. Divol, A. J. Kemp, C. Bellei, M. M. Marinak, and M. H. Key, "Fast-ignition transport studies: Realistic electron source, integrated particle-in-cell and hydrodynamic modeling, imposed magnetic fields," *Phys. Plasmas* **19**, 072711 (2012).
- <sup>25</sup>L. J. Perkins, B. G. Logan, G. B. Zimmerman, and C. J. Werner, "Two-dimensional simulations of thermonuclear burn in ignition-scale inertial confinement fusion targets under compressed axial magnetic fields," *Phys. Plasmas* **20**, 072708 (2013).
- <sup>26</sup>A. B. Sefkow and M. C. Herrmann, *Ignition Scaling Laws for Inertial Confinement Fusion. Part I: Spherical Targets Revisited* (Internal Sandia National Laboratories, 2024).
- <sup>27</sup>A. B. Sefkow, J. G. Shaw, A. J. Kish, M. J. Lavell, A. T. Sexton, S. Borve, A. Bowman, M. Burns, J. Carroll-Nellenback, S. A. Cohen *et al.*, "Overview of TriForce: Projects, progress, and plans," in *63rd Annual Meeting of the Division of Plasma Physics*, Pittsburgh, PA, 8–12 November 2021 (Bulletin of the American Physical Society, 2021).
- <sup>28</sup>J. I. Castor, *Radiation Hydrodynamics* (Cambridge University Press, 2007).
- <sup>29</sup>P. A. Sterne, L. X. Benedict, S. Hamel, A. A. Correa, J. L. Milovich, M. M. Marinak, P. M. Celliers, and D. E. Fratanduono, "Equations of state for ablator materials in inertial confinement fusion simulations," *J. Phys.: Conf. Ser.* **717**, 012082 (2016).
- <sup>30</sup>E. M. Epperlein and M. G. Haines, "Plasma transport coefficients in a magnetic field by direct numerical solution of the Fokker-Planck equation," *Phys. Fluids* **29**, 1029–1041 (1986).
- <sup>31</sup>M. Geissel, T. J. Awe, D. E. Bliss, E. M. Campbell, M. R. Gomez, E. Harding, A. J. Harvey-Thompson, S. B. Hansen, C. Jennings *et al.*, "Nonlinear laser-plasma interaction in magnetized liner inertial fusion," *Proc. SPIE* **9731**, 973100 (2016).